

Operator learning approach for the limited view problem in photoacoustic tomography *

Florian Dreier, Sergiy Pereverzyev Jr.[†] and Markus Haltmeier

October 9, 2018

Abstract

In photoacoustic tomography, one is interested to recover the initial pressure distribution inside a tissue from the corresponding measurements of the induced acoustic wave on the boundary of a region enclosing the tissue. In the limited view problem, the wave boundary measurements are given on the part of the boundary, whereas in the full view problem, the measurements are known on the whole boundary. For the full view problem, there exist various fast and robust reconstruction methods. These methods give severe reconstruction artifacts when they are applied directly to the limited view data. One approach for reducing such artefacts is trying to extend the limited view data to the whole region boundary, and then use existing reconstruction methods for the full view data. In this paper, we propose an operator learning approach for constructing an operator that gives an approximate extension of the limited view data. We consider the behavior of a reconstruction formula on the extended limited view data that is given by our proposed approach. Approximation errors of our approach are analyzed. We also present numerical results with the proposed extension approach supporting our theoretical analysis.

Keywords: photoacoustic tomography, wave equation, limited view problem, inversion formula, universal back-projection, data extension, operator learning.

AMS subject classifications: 65R32, 35L05, 92C55.

1 Introduction

Photoacoustic tomography (PAT) is an emerging non-invasive imaging technique. It is based on the photoacoustic effect, and it has a big potential for a successful use in biomedical studies, including preclinical research and clinical practice. Applications include tumor

*Department of Mathematics, University of Innsbruck, Technikerstraße 13, A-6020 Innsbruck, Austria, E-mail: florian.dreier@student.uibk.ac.at, sergiy.pereverzyev@uibk.ac.at, markus.haltmeier@uibk.ac.at

[†]from March 1, 2018 at the Department of Neuroradiology, Medical University of Innsbruck, Anichstraße 35, A-6020 Innsbruck, Austria, E-mail: sergiy.pereverzyev@i-med.ac.at

angiogenesis monitoring, blood oxygenation mapping, functional brain imaging, and skin melanoma detection [49, 31, 5, 47]

The principle of PAT is the following. When short pulses of non-ionising electromagnetic energy are delivered into a biological (semi-transparent) tissue, then parts of the electromagnetic energy become absorbed. The absorbed energy leads to a nonuniform thermoelastic expansion depending on the tissue structure. This gives rise to an initial acoustic pressure distribution, which further is the source of an acoustic pressure wave. These waves are detected by a measurement device on the boundary of the tissue. The mathematical task in PAT is to reconstruct the spatially varying initial pressure distribution using these measurements. The values of the initial pressure distribution inside the tissue allow to make a judgment about the directly unseen structure of the tissue. For example, whether there are some abnormal formations inside the investigated tissue, such as a tumor.

Consider the part of the boundary of a region enclosing the tissue where the wave measurements are available. This part is called observation boundary. If the tissue is fully enclosed by the observation boundary, then one speaks about the full view problem. Otherwise, if some part of the tissue boundary is not accessible, then one has the so-called limited view problem (LVP). The LVP frequently arises in practice, for example in breast imaging (see, e.g., [50, 26]).

The LVP can be approached using iterative reconstruction algorithms (see, e.g., [39, 37, 23, 52, 25, 19, 42]). Although these algorithms can provide accurate reconstruction, they are computationally expensive and time consuming. Approaches for the full view problem, such as time reversal [7, 24], Fourier domain algorithms [16, 29, 51], explicit reconstruction formulas [10, 9, 28, 30, 35], are faster than iterative reconstructions and additionally are robust and accurate. However, when they are directly applied on the limited view data, then one obtains severe reconstruction artifacts.

And so, an idea appears to try to extend the limited view data to the whole boundary, and then use efficient algorithms for the full view data on the extended data to obtain a reconstruction of the initial pressure. Knowing characterizations of the range of the forward operator, which maps the initial pressure distribution to the wave data on the whole boundary of the tissue, may be used for this purpose (see, e.g., [3, 11, 1, 26] and the references therein). This knowledge is expressed with so-called range conditions. In [40, 41], some of these conditions, the so-called moment conditions, were realized for the extension of the limited view data.

The data extension process based on the moment conditions is unstable, and therefore, mostly low frequencies of the limited view wave data can be extended. This instability is connected with the following issue. The observation boundary defines a so-called detection region, which, for typical measurement configurations, is the convex hull of the observation boundary [27]. It is known (see, e.g., [27, 44, 26]) that if the support of the initial pressure is contained in this detection region, then a stable recovery of the initial pressure from the limited view wave data is theoretically possible. However, the data extension process based on the moment conditions does not use information about the support of the initial pressure, and so, it does not employ advantages of the possible stable recovery.

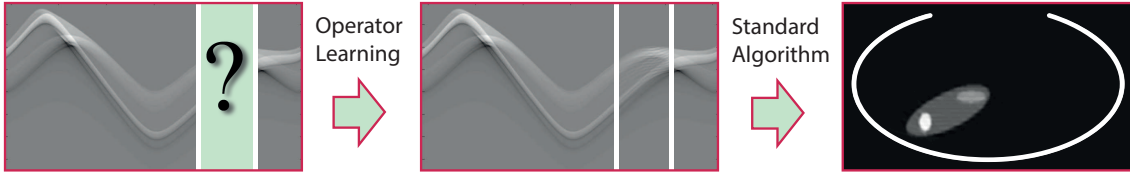


Figure 1: Illustration of the proposed approach for limited view PAT. In the first step, we extend the limited view data to the whole boundary via operator learning. In the second step, we apply a standard direct PAT reconstruction algorithm to the completed data.

In this paper, we propose a stable method for the extension of the limited view wave data that uses advantages of the mentioned possible stable recovery. Our method is based on the observation that in the case of the stable recovery, there exists a continuous data extension operator that maps the limited view wave data to the unknown wave data on the unobservable part of the boundary. We formally define this operator in Section 3.1. However, this operator is not explicitly known. In our method, we therefore propose to construct an approximate data extension operator using an operator learning approach that is inspired by the methods of the statistical learning theory (see, e.g., [22]). We suggest an operator learning procedure that uses the projection on the linear subspace defined by the training inputs.

Having an approximately extended limited view wave data, one can employ reconstruction methods for the full view wave data, such as time reversal or methods based on the explicit inversion formulas. As an example, we consider an explicit reconstruction formula for that purpose. We demonstrate that the resulting reconstruction algorithm corrects most limited view reconstruction artifacts, while the computational time remains to be low. The involved steps in the proposed reconstruction approach are illustrated in Figure 1.

The rest of the paper is organized as follows. In section 2, we present a mathematical background for PAT, give the used explicit reconstruction formula, and discuss the LVP. Our operator learning approach to the extension of the limited view wave data is given in section 3. In section 4, we analyze the approximation errors of our approach. We look at the approximation errors for the unknown wave data and for the corresponding reconstructions obtained by explicit reconstruction formulas. We present the numerical results in section 5. Finally, we finish the paper with conclusion and outlook in section 6.

2 Mathematics of PAT

Let $\Omega \subseteq \mathbb{R}^d$ be a bounded domain with a smooth boundary $\partial\Omega$, where $d \geq 2$ denotes the spatial dimension. Further, let $C_c^\infty(\Omega)$ be the set of all smooth functions $f: \mathbb{R}^d \rightarrow \mathbb{R}$ that are compactly supported in Ω . In PAT, one is interested to recover an unknown function $f \in C_c^\infty(\Omega)$ from the solution of the wave equation given on the boundary of Ω . Let us mathematically specify this reconstruction problem.

2.1 Reconstruction problem

Let $\mathfrak{U}f: \mathbb{R}^d \times (0, \infty) \rightarrow \mathbb{R}$ denote the solution of the following initial value problem for the wave equation:

$$\begin{cases} (\partial_t^2 - \Delta_x) u(x, t) = 0 & \text{for } (x, t) \in \mathbb{R}^d \times (0, \infty), \\ u(x, 0) = f(x) & \text{for } x \in \mathbb{R}^d, \\ (\partial_t u)(x, 0) = 0 & \text{for } x \in \mathbb{R}^d. \end{cases} \quad (1)$$

Here ∂_t denotes differentiation with respect to the second variable t , and Δ_x is the Laplacian with respect to x . Then the reconstruction problem in PAT consists in recovering the unknown function $f \in C_c^\infty(\Omega)$ from the corresponding wave boundary data

$$u(x, t) = (\mathfrak{U}f)(x, t) \quad \text{for } (x, t) \in \Gamma_1 \times (0, \infty), \quad (2)$$

where $\Gamma_1 \subseteq \partial\Omega$. If $\Gamma_1 = \partial\Omega$, then (2) is called full view problem; otherwise, if $\Gamma_1 \subsetneq \partial\Omega$, we have the limited view problem (LVP). In this paper, we are particularly interested in the limited view case, which we consider in some detail in subsection 2.3.

Let us denote the unobservable part of the boundary as $\Gamma_2 := \partial\Omega \setminus \Gamma_1$. We define also the following restrictions of $\mathfrak{U}f$:

$$\mathcal{U}f := \mathfrak{U}f|_{\partial\Omega \times (0, \infty)}, \quad \mathcal{U}_1 f := \mathfrak{U}f|_{\Gamma_1 \times (0, \infty)}, \quad \mathcal{U}_2 f := \mathfrak{U}f|_{\Gamma_2 \times (0, \infty)}. \quad (3)$$

Let us note that in practice, the reconstruction problem (2) arises in PAT in spatial dimensions two and three. The three dimensional problem appears when the so-called point-like detectors are used (see, for example, [49, 27, 12]). When one uses linear or circular integrating detectors, then the reconstruction problem (2) is considered in two spatial dimensions (see [6, 15, 38, 53]).

2.2 Explicit inversion formula

The reconstruction problem (2) can be approached by various solution techniques. Among these techniques, the derivation of the explicit inversion formulas of the so-called back-projection type is particularly appealing. A numerical realization of these formulas typically gives reconstruction algorithms that are accurate and robust, and at the same time are faster than iterative approaches.

An inversion formula consists of an explicitly given operator \mathcal{G}_d that recovers the function f from the data u . Such formulas are currently known only for special domains and only for the full view data, i.e. u must be given for all $x \in \partial\Omega$. In this paper, we consider the formula that first has been derived in [48, 28, 6]. In addition to the data u , the formula \mathcal{G}_d also depends on the boundary $\partial\Omega$ of the domain $\Omega \subsetneq \mathbb{R}^d$ and on the reconstruction point $x_0 \in \Omega$. The structure of the formula further depends on whether the spatial dimension d is even or odd.

If $d \geq 2$ is an even integer, then

$$\mathcal{G}_d(\partial\Omega, u, x_0) := \kappa_d \int_{\partial\Omega} \langle \nu_x, x_0 - x \rangle \int_{|x_0-x|}^{\infty} \frac{(\partial_t \mathcal{D}_t^{(d-2)/2} t^{-1} u)(x, t)}{\sqrt{t^2 - |x_0 - x|^2}} dt ds(x). \quad (4)$$

Here $\kappa_d := (-1)^{(d-2)/2} / \pi^{d/2}$ is a constant, ν_x denotes the outward pointing unit normal to $\partial\Omega$, and $\mathcal{D}_t := (2t)^{-1} \partial_t$ is the differentiation operator with respect to t^2 . Further, $\langle \cdot, \cdot \rangle$ and $|\cdot|$ denote the standard inner product and the corresponding Euclidian norm on \mathbb{R}^d , respectively.

In the case of odd dimension $d \geq 3$, the formula \mathcal{G}_d is defined as follows:

$$\mathcal{G}_d(\partial\Omega, u, x_0) := \kappa_d \int_{\partial\Omega} \frac{\langle \nu_x, x_0 - x \rangle}{|x_0 - x|} (\partial_t \mathcal{D}_t^{(d-3)/2} t^{-1} u)(x, |x_0 - x|) ds(x), \quad (5)$$

with constant $\kappa_d := (-1)^{(d-3)/2} / (2\pi^{(d-1)/2})$.

The formula \mathcal{G}_d has been introduced in [48] for dimension $d = 3$, and in [6] for dimension $d = 2$. In [28], it has been studied for the case when Ω is a ball in arbitrary dimension. Further, in [34, 17, 18], it has been shown that for any elliptical domain Ω , the formula \mathcal{G}_d exactly recovers any smooth function f with support in Ω from data $u = \mathcal{U}f$. In [20], it was shown, that the same result also holds for parabolic domains Ω with $d = 2$. The formula \mathcal{G}_d in arbitrary spatial dimension $d \geq 2$ on certain quadric hypersurfaces, including the parabolic ones, has been analyzed in [21].

It should be noted that the formula \mathcal{G}_d can be in fact used for any convex bounded domain Ω . Then, however, the formula does not recover the function f exactly, and it introduces an approximation error. The form of this error has been analyzed in [34, 17, 18]. Numerical experiments indicate that this error is rather low for domains that can be well approximated by elliptic domains. This is also suggested by the microlocal analysis in [35].

The operator \mathcal{U} can be defined for functions $f \in \mathcal{L}^2(\Omega_0)$, where Ω_0 is an open set with $\overline{\Omega_0} \subseteq \Omega$. Define the image of $\mathcal{L}^2(\Omega_0)$ under the operator \mathcal{U} as $\mathbb{Y} := \mathcal{U}(\mathcal{L}^2(\Omega_0))$. Then it is known (see, e.g., [27, 44, 26]) that \mathbb{Y} is a closed subspace of $\mathcal{L}^2(\partial\Omega \times (0, \infty))$, and therefore, we will treat \mathbb{Y} as a Hilbert space with the scalar product of $\mathcal{L}^2(\partial\Omega \times (0, \infty))$. Moreover, the operator $\mathcal{U}: \mathcal{L}^2(\Omega_0) \rightarrow \mathbb{Y}$ is bounded, and it has the bounded inverse $\mathcal{U}^{-1}: \mathbb{Y} \rightarrow \mathcal{L}^2(\Omega_0)$.

In the following, we will work with functions $f \in \mathcal{L}^2(\Omega_0)$, and we will assume that the domain Ω is such that the formula \mathcal{G}_d gives exact recovery of the function f from its wave data $u = \mathcal{U}f$, i.e. it holds that

$$f = \mathcal{G}_d \mathcal{U}f. \quad (6)$$

As we already mentioned, this is, for example, the case for circular and elliptical domains. In such a situation, it can be shown that \mathcal{G}_d is a continuous extension of \mathcal{U}^{-1} to $\mathcal{L}^2(\partial\Omega \times (0, \infty))$.

2.3 Limited view problem

In practice, the wave data u is frequently given on a subset Γ_1 of the boundary $\partial\Omega$ (Figure 2). This subset Γ_1 , called observation boundary, defines the so-called detection region

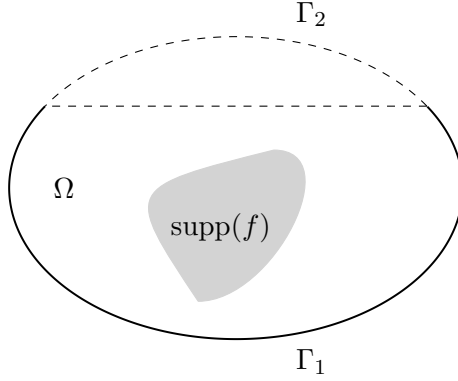


Figure 2: Setting of LVP.

$\mathbb{D}(\Gamma_1)$ (see, e.g., [37, 27]). If $\overline{\text{supp}(f)} \not\subseteq \mathbb{D}(\Gamma_1)$, then the function f in (2) can be stably recovered from data on Γ_1 . The detection region $\mathbb{D}(\Gamma_1)$ contains points x such that any line going through x intersects Γ_1 . For example, if Γ_1 is a spherical or elliptical cap, then $\mathbb{D}(\Gamma_1) = \text{conv}(\Gamma_1)$.

Let us mathematically specify the stable recovery of f . Let Ω_1 be an open set with $\overline{\Omega_1} \not\subseteq \mathbb{D}(\Gamma_1)$. The stable recovery holds for $f \in \mathcal{L}^2(\Omega_1)$, and it is formulated in the following theorem. Note that the space $\mathcal{L}^2(\Omega_1)$ is identified with the set of all functions in $\mathcal{L}^2(\mathbb{R}^d)$ that vanish outside of $\overline{\Omega_1}$.

Theorem 1. *The operator $\mathcal{U}_1: \mathcal{L}^2(\Omega_1) \rightarrow \mathcal{L}^2(\Gamma_1 \times (0, \infty))$ is well defined and bounded. Moreover, it has bounded inverse $\mathcal{U}_1^{-1}: \mathbb{Y}_1 \rightarrow \mathcal{L}^2(\Omega_1)$, where $\mathbb{Y}_1 := \mathcal{U}_1(\mathcal{L}^2(\Omega_1)) \subseteq \mathcal{L}^2(\Gamma_1 \times (0, \infty))$ denotes the range of \mathcal{U}_1 . In particular, \mathbb{Y}_1 is closed.*

Proof. It is sufficient to show the two-side estimate

$$\forall f \in C_c^\infty(\Omega_1): \quad a \|\mathcal{U}_1 f\|_{\mathcal{L}^2} \leq \|f\|_{\mathcal{L}^2} \leq b \|\mathcal{U}_1 f\|_{\mathcal{L}^2}, \quad (7)$$

for some constants $a, b \in (0, \infty)$. The claims then follow by continuous extension.

To show the left hand estimate, we decompose $\mathcal{U}_1 f = \chi_{[0, T]} \mathcal{U}_1 f + \chi_{(T, \infty)} \mathcal{U}_1 f$, where T is larger than the diameter of Ω . Since the operator \mathcal{U}_1 is the sum of two Fourier integral operators of order zero (see [19]), we have $\|\chi_{[0, T]} \mathcal{U}_1 f\|_{\mathcal{L}^2} \leq c_1 \|f\|_{\mathcal{L}^2}$ for some constant c_1 . Moreover, the explicit formulas for $\mathcal{U}_1 f$ (see, e.g., [8]) imply also that $\|\chi_{(T, \infty)} \mathcal{U}_1 f\|_{\mathcal{L}^2} \leq c_1 \|f\|_{\mathcal{L}^2}$, which gives the left hand side estimate in (7).

The right hand side estimate can be found in [19, Theorem 3.4]. The required visibility condition is satisfied for $f \in \mathcal{L}^2(\Omega_1)$. \square

It is worth to mention that despite the boundedness of \mathcal{U}_1^{-1} , no theoretically exact direct solution methods are available. Let us note that if the condition $\overline{\Omega_1} \not\subseteq \mathbb{D}(\Gamma_1)$ is not satisfied, then the visibility condition in [19, Theorem 3.4] is also not valid, and the inverse of the operator \mathcal{U}_1 is severely ill-posed (see, e.g., [19, 44, 26]).

Denote $\mathbb{Y}_2 := \mathcal{L}^2(\Gamma_2 \times (0, \infty))$. From the boundness of the operator $\mathcal{U}: \mathcal{L}^2(\Omega_0) \rightarrow \mathbb{Y}$, we can deduce the boundness of the operator $\mathcal{U}_2: \mathcal{L}^2(\Omega_1) \rightarrow \mathbb{Y}_2$. We will use this for the data extension operator below.

Recall that in order to give the exact reconstruction, the formula \mathcal{G}_d requires the full view wave data u , which is given for all $x \in \partial\Omega$ (see (6)). In spite of the above discussed stable recoverability of $f \in \mathcal{L}^2(\Omega_1)$ from equation (2), the use of formula \mathcal{G}_d on the limited view data u given on $\Gamma_1 \subsetneq \partial\Omega$ leads to serious artifacts in the reconstruction; see, e.g., [20], where the numerical results of the application of \mathcal{G}_2 on finite parabolas are presented. The reconstruction artefacts in the case of the limited view data are also discussed in [50, 13, 45, 4, 14, 36].

At the same time, the use of formula \mathcal{G}_d for reconstructing function f can be attractive from various points of view. For example, as we already pointed out, the reconstruction using a numerical realization of \mathcal{G}_d is faster than iterative reconstruction algorithms. Another point may be connected with the nature of the software development. Namely, having already a tested and trusted computer code of the numerical realization of formula \mathcal{G}_d , it could be tempting to develop its extensions for the LVP.

An extension of the limited view data u from the observable part of the boundary $\Gamma_1 \subsetneq \partial\Omega$ to the whole boundary $\partial\Omega$ may give a possibility to improve the reconstruction quality of the formula \mathcal{G}_d . In this paper, we propose to realize this extension using the operator learning approach, which we consider in the next section.

3 Data extension using operator learning approach

The extension of the limited view data to the whole boundary can be in principle done by the extension operator that we define in the next subsection. This operator is however not explicitly known, and we propose an operator learning approach to construct its approximation in subsection 3.2. In subsection 3.3, we discuss computational aspects of the proposed learned approximation of the extension operator.

3.1 Extension operator

Let us recall that $\Gamma_1 \subsetneq \partial\Omega$ is the observation boundary, $\mathbb{D}(\Gamma_1)$ is the corresponding detection region defined in Section 2.3, $\Gamma_2 = \partial\Omega \setminus \Gamma_1$ is the unobservable part of the boundary, and Ω_1 is an open set with $\overline{\Omega_1} \subsetneq \mathbb{D}(\Gamma_1)$. Further, let us remind that the operators \mathcal{U}_1 and \mathcal{U}_2 are defined in (3).

The operator $\mathcal{A}: \mathbb{Y}_1 \rightarrow \mathbb{Y}_2$ that maps functions $\mathcal{U}_1 f$ to functions $\mathcal{U}_2 f$ for $f \in \mathcal{L}^2(\Omega_1)$ realizes the extension of the limited view data $u_1 = \mathcal{U}_1 f$ to the unobservable part of the boundary Γ_2 . This operator \mathcal{A} can be written as $\mathcal{A} = \mathcal{U}_2 \circ \mathcal{U}_1^{-1}$. Because of this representation and the assumptions on Γ_1 and Ω_1 , the operator \mathcal{A} is a linear continuous operator as a superposition of linear continuous operators. Recall that the continuity (or boundness) of the operators \mathcal{U}_1^{-1} and \mathcal{U}_2 is discussed in Section 2.3.

With the introduced extension operator \mathcal{A} , one could extend the limited view data u_1 to

the whole boundary $\partial\Omega$, and then use the formula \mathcal{G}_d on this extended data. In this way, the disadvantages of the use of the formula \mathcal{G}_d on the limited view data can be eliminated. However, the form of the operator \mathcal{A} is not explicitly known.

3.2 Proposed learned extension operator

In this paper, we propose to construct an operator $\hat{\mathcal{A}}_n$ that approximates the operator \mathcal{A} . The role of the parameter $n \in \mathbb{N} \cup \{0\}$ is described below. The approximate operator $\hat{\mathcal{A}}_n$ must satisfy the following two requirements. The first requirement concerns the approximation quality: $\hat{\mathcal{A}}_n u_1$ must be close to $\mathcal{A}u_1$. The second requirement is related to the computational effort of the numerical evaluation of $\hat{\mathcal{A}}_n u_1$. This evaluation must be fast such that the evaluation of the formula \mathcal{G}_d on the extended limited view data with the help of $\hat{\mathcal{A}}_n$ remains to be computationally efficient.

Our construction of the approximate operator $\hat{\mathcal{A}}_n$ is inspired by the statistical learning approach (see, e.g., [22]). For $i = 1, \dots, n$, consider training functions $f_i: \Omega_1 \rightarrow \mathbb{R}$. For each training function f_i , we can determine the corresponding wave data $u_{1,i} := \mathcal{U}_1 f_i$, $u_{2,i} := \mathcal{U}_2 f_i$. By the definition of the extension operator \mathcal{A} we have that $u_{2,i} = \mathcal{A}u_{1,i}$. In the context of statistical learning, the set $\mathcal{Z} := \{(u_{1,i}, \mathcal{A}u_{1,i}), i = 1, \dots, n\}$ is called a training set. Define for future reference the set $\mathbf{U}_{1,n} := \{u_{1,i}, i = 1, \dots, n\}$.

So, how to construct (or, using the terminology of the statistical learning, how to learn) an approximation $\hat{\mathcal{A}}_n u_1$ of $\mathcal{A}u_1$ using the training set \mathcal{Z} ? It should be noted that many statistical learning algorithms are designed for learning a small number of scalar-valued functions. These algorithms are not applicable in our case because the function that we need to learn is an operator. Recently, the development of the statistical learning methods for learning vector-valued functions and also functions with values in function spaces, i.e. operators, has been started (see, e.g., [33, 2]). For obtaining good results, these methods require an a priori knowledge of the dependence between different components of the output vector that is given by the function to be learned. This knowledge is not readily available in our case. However, as we observe below, the linear structure of the extension operator \mathcal{A} that we want to learn allows to employ a projection operator for the learning.

For any $n \in \mathbb{N} \cup \{0\}$, define the linear subspace

$$V_n := \left\{ \sum_{j=1}^n c_j u_{1,j}, c_j \in \mathbb{R} \right\}, V_0 := \{0\} \subseteq \mathbb{Y}_1, \quad (8)$$

and let $\mathcal{P}_n: \mathcal{L}^2(\Gamma_1 \times (0, \infty)) \rightarrow V_n$ be the orthogonal projection on V_n in $\mathcal{L}^2(\Gamma_1 \times (0, \infty))$. Then we define the learned approximation $\hat{\mathcal{A}}_n u_1$ as follows:

$$\hat{\mathcal{A}}_n u_1 := \mathcal{A} \mathcal{P}_n u_1. \quad (9)$$

Note that $V_n \subseteq \mathbb{Y}_1$, and therefore, the operator composition $\mathcal{A} \mathcal{P}_n$ is well-defined, and $\hat{\mathcal{A}}_n: \mathcal{L}^2(\Gamma_1 \times (0, \infty)) \rightarrow \mathbb{Y}_2$ is bounded. Further, note that for all $u_1 \in \mathcal{L}^2(\Gamma_1 \times (0, \infty))$, $\hat{\mathcal{A}}_0 u_1 = 0 \in \mathbb{Y}_2$.

3.3 Computation of learned approximation

How to compute the learned approximation $\hat{\mathcal{A}}_n u_1$ using the training set \mathcal{Z} for $n \geq 1$? First of all, observe that since $\mathcal{P}_n u_1 \in V_n$, the projection $\mathcal{P}_n u_1$ has the following representation:

$$\mathcal{P}_n u_1 = \sum_{j=1}^n c_j u_{1,j}, \quad (10)$$

where the coefficients $c_j \in \mathbb{R}$ can be determined from the conditions $\langle \mathcal{P}_n u_1 - u_1, u_{1,i} \rangle = 0$ for $i = 1, \dots, n$. These conditions can be written in the form of the system of linear equations for the coefficients c_j

$$\sum_{j=1}^n c_j \langle u_{1,i}, u_{1,j} \rangle = \langle u_1, u_{1,i} \rangle, \quad i = 1, \dots, n. \quad (11)$$

Denote the matrix corresponding to the above linear system as \mathbf{P}_n , i.e. the elements of \mathbf{P}_n are $(\mathbf{P}_n)_{ij} = \langle u_{1,i}, u_{1,j} \rangle$. Further, denote the vector of unknowns as \mathbf{c}_n , and the right-hand side as \mathbf{u}_n , i.e. $(\mathbf{c}_n)_i = c_i$ and $(\mathbf{u}_n)_i = \langle u_1, u_{1,i} \rangle$.

The matrix \mathbf{P}_n is the Gram matrix of the functions in $\mathbf{U}_{1,n}$, and it is invertible if the set $\mathbf{U}_{1,n}$ is linearly independent. Since the operator \mathcal{U}_1 is invertible, the set $\mathbf{U}_{1,n}$ is linearly independent if the set $\{f_i, i = 1, \dots, n\}$ is linearly independent, and for the following, we assume that this is the case.

Note that the matrix \mathbf{P}_n does not depend on the limited view wave data u_1 that we want to extend. Therefore, the inverse matrix \mathbf{P}_n^{-1} can be precomputed once the set of the learning inputs $\mathbf{U}_{1,n}$ is given. This will make the determination of the coefficients c_j very fast.

Finally, with the coefficients c_j in (10), i.e. $\mathbf{c}_n = \mathbf{P}_n^{-1} \mathbf{u}_n$, the approximation $\hat{\mathcal{A}}_n u_1$ is calculated as follows:

$$\hat{\mathcal{A}}_n u_1 = \mathcal{A} \mathcal{P}_n u_1 = \mathcal{A} \left(\sum_{j=1}^n c_j u_{1,j} \right) = \sum_{j=1}^n c_j u_{2,j} = \sum_{j=1}^n c_j \mathcal{U}_2 f_j.$$

4 Approximate reconstructions and their error analysis

For obtaining an approximate reconstruction of f using the limited view data $u_1 = \mathcal{U}_1 f$ and the formula \mathcal{G}_d , we can now proceed as follows. First, we extend the limited view data u_1 to the whole boundary $\partial\Omega$ using the learned extension operator $\hat{\mathcal{A}}_n$ in this way:

$$\hat{u}_n(x, t) = \begin{cases} u_1(x, t) & \text{if } x \in \Gamma_1, \\ (\hat{\mathcal{A}}_n u_1)(x, t) & \text{if } x \in \Gamma_2. \end{cases}$$

And then we apply the formula \mathcal{G}_d to this extended wave data \hat{u}_n in order to obtain an approximate reconstruction \hat{f}_n :

$$\hat{f}_n = \mathcal{G}_d \hat{u}_n. \quad (12)$$

Note that \hat{u}_0 is obtained by extending the limited view data u_1 to the whole boundary $\partial\Omega$ with zero values on Γ_2 . As we already discussed, the corresponding approximate reconstruction \hat{f}_0 contains significant errors, and it is desirable to have better reconstructions of f using u_1 . Additionally, one may desire that the reconstruction \hat{f}_n improves as n increases.

In the following theorem, we estimate the \mathcal{L}^2 -error of the approximation of $\mathcal{A}u_1$ by $\hat{\mathcal{A}}_n u_1$ and of the approximation of f by \hat{f}_n . From the derived estimates, we see that the above aims can be realized if the training functions $f_i, i = 1, \dots, n$, are chosen appropriately.

Theorem 2. *Let a set of linearly independent training functions $\{f_i, i = 1, \dots, n\} \subseteq \mathcal{L}^2(\Omega_1)$ be given, and denote $W_n := \{\sum_{i=1}^n c_i f_i, c_i \in \mathbb{R}\}$, $W_0 := \{0\} \subseteq \mathcal{L}^2(\Omega_1)$. Define the training limited view wave data $u_{1,i} := \mathcal{U}_1 f_i$, the corresponding linear subspace V_n in (8), and the learned extension operator $\hat{\mathcal{A}}_n$ in (9). Consider a function $f \in \mathcal{L}^2(\Omega_1)$, its limited view wave data $u_1 := \mathcal{U}_1 f$, and its approximation \hat{f}_n defined in (12). Then the following \mathcal{L}^2 -error estimate for the unobservable data holds:*

$$\left\| \mathcal{A}u_1 - \hat{\mathcal{A}}_n u_1 \right\| \leq \|\mathcal{A}\| \cdot \|\mathcal{U}_1\| \cdot \min_{g \in W_n} \|f - g\|. \quad (13)$$

If additionally, the domain Ω is such that (6) holds, then we have the following \mathcal{L}^2 -error estimate for the reconstruction:

$$\left\| f - \hat{f}_n \right\| \leq \|\mathcal{G}_d\| \cdot \|\mathcal{A}\| \cdot \|\mathcal{U}_1\| \cdot \min_{g \in W_n} \|f - g\|. \quad (14)$$

Proof. We first prove (13). From the definition of the operator $\hat{\mathcal{A}}_n$, we have that

$$\left\| \mathcal{A}u_1 - \hat{\mathcal{A}}_n u_1 \right\| = \|\mathcal{A}\mathcal{U}_1 f - \mathcal{A}\mathcal{P}_n \mathcal{U}_1 f\| \leq \|\mathcal{A}\| \cdot \|\mathcal{U}_1 f - \mathcal{P}_n \mathcal{U}_1 f\|. \quad (15)$$

From the properties of the projection operators, we also have that

$$\|\mathcal{U}_1 f - \mathcal{P}_n \mathcal{U}_1 f\| = \min_{h \in V_n} \|\mathcal{U}_1 f - h\|. \quad (16)$$

For an element $h \in V_n$, there are unique constants $c_i \in \mathbb{R}, i = 1, \dots, n$ such that

$$h = \sum_{i=1}^n c_i u_{1,i} = \sum_{i=1}^n c_i \mathcal{U}_1 f_i = \mathcal{U}_1 \left(\sum_{i=1}^n c_i f_i \right),$$

and therefore, there exists an element $g \in W_n$ such that $h = \mathcal{U}_1 g$. Using this fact, we can estimate

$$\min_{h \in V_n} \|\mathcal{U}_1 f - h\| = \min_{g \in W_n} \|\mathcal{U}_1 f - \mathcal{U}_1 g\| \leq \|\mathcal{U}_1\| \cdot \min_{g \in W_n} \|f - g\|. \quad (17)$$

Then combining (15),(16),(17), we obtain estimate (13) for the \mathcal{L}^2 -error $\|\mathcal{A}u_1 - \hat{\mathcal{A}}_n u_1\|$.

Now, consider (14). Using (6) and (12), we have

$$\left\| f - \hat{f}_n \right\| = \|\mathcal{G}_d \mathcal{U} f - \mathcal{G}_d \hat{u}_n\| \leq \|\mathcal{G}_d\| \cdot \|\mathcal{U} f - \hat{u}_n\|. \quad (18)$$

Since $(\mathcal{U}f)(x, t) = \hat{u}_n(x, t) = u_1(x, t)$ for $x \in \Gamma_1$, then

$$\|\mathcal{U}f - \hat{u}_n\| = \|\mathcal{U}_2f - \hat{\mathcal{A}}_n u_1\| = \|\mathcal{A}u_1 - \hat{\mathcal{A}}_n u_1\|. \quad (19)$$

Thus, the error estimate (14) is obtained from (18), (19), and the error estimate (13). \square

Remark 1. Let $\mathcal{Q}_n: \mathcal{L}^2(\Omega_1) \rightarrow W_n$ be the orthogonal projection on W_n in the space $\mathcal{L}^2(\Omega_1)$. Then, since we have that $\min_{g \in W_n} \|f - g\| = \|f - \mathcal{Q}_n f\|$, we can write $\|f - \mathcal{Q}_n f\|$ instead of $\min_{g \in W_n} \|f - g\|$ in (13) and (14).

As we see from Theorem 2, the estimates of the \mathcal{L}^2 -errors given by our learning procedure depend on the minimal distance from the unknown function f to the linear subspace W_n defined by the training functions f_i . This gives us an indication for the choice of the training functions. Namely, one should choose the training functions f_i such that the unknown function f can be well approximated by their linear combination.

Estimates (13),(14) also allow us to state the condition for the exact approximation given by our learning procedure and for the convergence of the learned approximation when the number of the training functions n goes to infinity. We present these conditions in the following two corollaries.

Corollary 1. If $f \in W_n$, then the learned approximation $\hat{\mathcal{A}}_n u_1$ and the reconstruction \hat{f}_n are exact, i.e.

$$\|\mathcal{A}u_1 - \hat{\mathcal{A}}_n u_1\| = \|f - \hat{f}_n\| = 0.$$

Corollary 2. If $\overline{\bigcup_{n \geq 1} W_n} = \mathcal{L}^2(\Omega_1)$, then the learned approximation $\hat{\mathcal{A}}_n u_1$ and the reconstruction \hat{f}_n converge respectively to $\mathcal{A}u_1$ and f as $n \rightarrow \infty$, i.e.

$$\lim_{n \rightarrow \infty} \|\mathcal{A}u_1 - \hat{\mathcal{A}}_n u_1\| = \lim_{n \rightarrow \infty} \|f - \hat{f}_n\| = 0.$$

Let us now compare the errors of the approximations \hat{f}_n with $n \geq 1$ and \hat{f}_0 . The \mathcal{L}^2 -error estimates (13),(14) for $n = 0$ become:

$$\|\mathcal{A}u_1 - 0\| \leq \|\mathcal{A}\| \cdot \|\mathcal{U}_1\| \cdot \|f\|, \quad (20)$$

$$\|f - \hat{f}_0\| \leq \|\mathcal{G}_d\| \cdot \|\mathcal{A}\| \cdot \|\mathcal{U}_1\| \cdot \|f\|. \quad (21)$$

Comparing the error estimates (13),(14) for the learned approximations with $n \geq 1$ and the error estimates (20),(21) for the approximations using zero extension of the limited view wave data, one sees that these error estimates differ regarding the following factors:

$$\mathcal{E}_n(f) := \min_{g \in W_n} \|f - g\|, \quad \mathcal{E}_0(f) := \|f\|, \quad (22)$$

correspondingly for learned approximations with $n \geq 1$ and approximation using zero extension.

The factors (22) can be seen as indicators for the expected approximation quality of the considered algorithms. For a fixed non-zero function f , the factor $\mathcal{E}_0(f)$ is a fixed non-zero value, while the factor $\mathcal{E}_n(f)$ can be zero, or can be made arbitrary small, see Corollaries 1,2. Therefore, the approximation quality of the learned approximations is expected to be better than of the approximations using zero extension of the data. This expectation will be confirmed by the numerical results in the next section. In fact, one can show (see Remark 2 below) that the factor $\mathcal{E}_n(f)$ is always less or equal than the factor $\mathcal{E}_0(f)$, and the strict inequality $\mathcal{E}_n(f) < \mathcal{E}_0(f)$ holds under rather mild conditions on the function f and the training functions f_i . Generally, this condition can be expected to hold in practice.

Remark 2. *Using properties of the projection operators in Hilbert spaces, one can show that the sequence $\mathcal{E}_n(f)$ is nonincreasing, i.e.*

$$\mathcal{E}_n(f) \leq \mathcal{E}_m(f) \quad \text{for } n > m \geq 0. \quad (23)$$

If additionally

$$\langle f, f_i \rangle \neq 0 \quad \text{for some } i \in \{m+1, \dots, n\}, \quad (24)$$

then inequality (23) is strict, i.e.

$$\mathcal{E}_n(f) < \mathcal{E}_m(f) \quad \text{for } n > m \geq 0. \quad (25)$$

Condition (24) is also necessary for (25), i.e. if (25) holds, then we have (24).

5 Numerical results

In this section, we present results of the numerical realization of the proposed operator learning approach.

We consider the spatial dimension $d = 2$, and we take the elliptical domain

$$\Omega = \left\{ (x_1, x_2) \in \mathbb{R}^2 \mid (x_1/a_1)^2 + (x_2/a_2)^2 < 1 \right\},$$

with $a_1 = 2$, $a_2 = 1$. We use the following parametrization of the boundary

$$\partial\Omega = \{ (a_1 \cos \theta, a_2 \sin \theta) \mid \theta \in [-\pi, \pi) \},$$

and we assume that the unobservable part of the boundary is (see Figure 3(left))

$$\Gamma_2 = \{ (a_1 \cos \theta, a_2 \sin \theta) \mid \theta \in [0.97, 2.17) \}.$$

Thus, approximately 19% of the angular values are missing.

We work with the function f presented in Figure 3(left). Its numerical full view wave boundary data $u = \mathcal{U}f$ is given in Figure 3(right), and we use the corresponding limited view wave boundary data $u_1 = \mathcal{U}_1 f$. The observation boundary Γ_1 is discretized such that the distance between two consecutive points is in the interval $[0.0099, 0.0101]$. We take the time step size as 0.01.

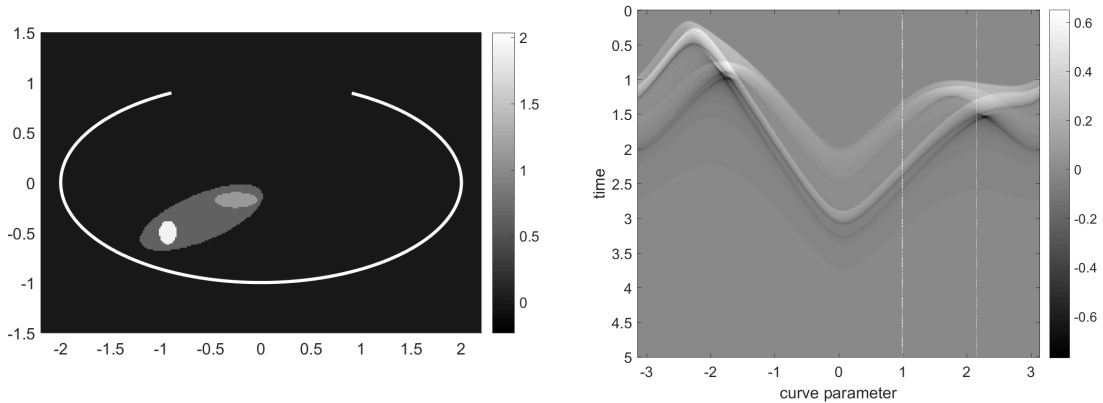


Figure 3: Left: the function f that we use in our numerical experiments and the chosen observation boundary Γ_1 . Right: the corresponding numerical full view wave boundary data $\mathcal{U}f$. The region between two white vertical lines corresponds to the unknown part of the data on the unobservable part of the boundary Γ_2 .

We further assume that we know a rectangular region

$$K = \{ (x_1, x_2) \in \mathbb{R}^2 \mid -1.25 \leq x_1 < 0.5, -0.7 \leq x_2 < 0.1752 \}$$

that contains the support of f (Figure 4(top and bottom)). We use this region K for defining training functions f_i . Namely, we consider partitions of the region K into squares K_i , $i \in \{1, \dots, n\}$. The square K_i contains points $(x_1, x_2) \in \mathbb{R}^2$ such that

$$\begin{aligned} -1.25 + ([i/n_h] - 1)w/n_w &\leq x_1 < -1.25 + [i/n_h]w/n_w, \\ -0.7 + (i \bmod n_h - 1)h/n_h &\leq x_2 < -0.7 + (i \bmod n_h)h/n_h, \end{aligned}$$

where $w = 1.75$ (width of K), $h = 0.8752$ (height of K), $n_w = \sqrt{2n}$, $n_h = n_w/2$ (see Figure 4(middle)). Then we define the training function f_i as the indicator function of the square K_i . We take the number of the training functions in the form $n = n_1 \times n_2$, where n_1 and n_2 are the numbers of the partitioning intervals along the coordinate x_1 and x_2 correspondingly. We present the numerical results for $n = 4 \times 2$, 8×4 , 16×8 , 32×16 .

Let us note that we use the rectangular region K for illustration purpose. If the region containing $\text{supp}(f)$ is not known, then one may consider squares filling the whole subset Ω_1 of the detection region $\mathbb{D}(\Gamma_1)$. Further note that other type of basis functions can be used in a similar manner. Kaiser-Bessel functions, which are frequently used in computed tomography (see, e.g., [32, 46, 43]), would be another reasonable choice.

The extended limited view data \hat{u}_n using the learned extension operator $\hat{\mathcal{A}}_n$ for the considered values of n are presented in Figure 5. We observe that as n increases, the extended data \hat{u}_n approaches the full view data u in Figure 3(right). Note that the chosen training functions f_i satisfy the condition of Corollary 2. Therefore, the approach of \hat{u}_n to the full view data u is in agreement with our theoretical analysis.

The reconstructions \hat{f}_n using the extended data \hat{u}_n are presented in Figure 6(2nd and 3rd rows). For comparison purpose, we also present the reconstruction \hat{f} using the full

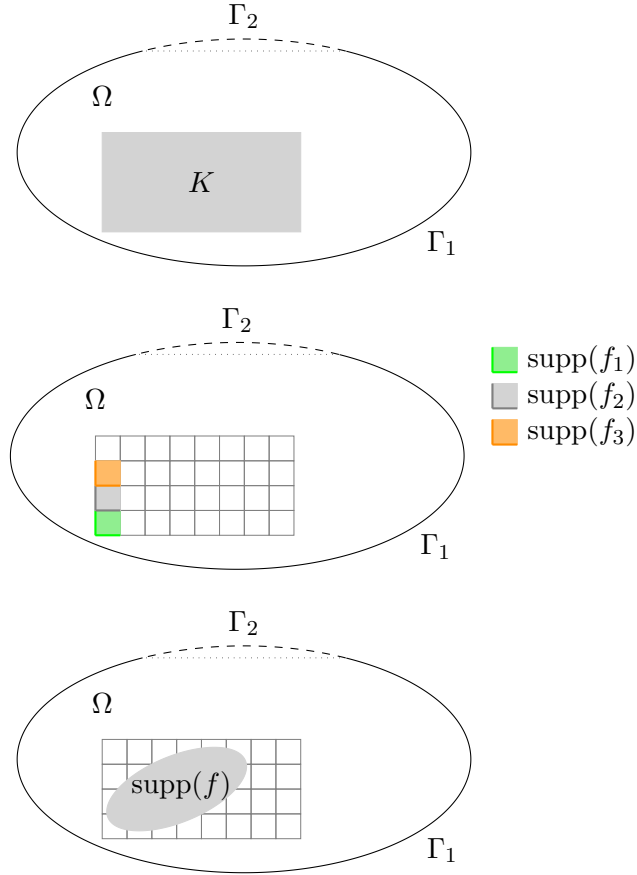


Figure 4: Top: the rectangular region K containing $\text{supp}(f)$. Middle: the example of the partition of K into 8×4 squares. The training functions f_i are numbered starting from the bottom-left square from bottom to top and from left to right. Bottom: the position of $\text{supp}(f)$ in K with the partition of K into 8×4 squares.

view wave boundary data u , and the reconstruction \hat{f}_0 using the zero extended data \hat{u}_0 (Figure 6(1st row)). We evaluate the reconstructions at the points from the discrete set

$$\Omega_h := \{ (-2.2 + n_1 h, -2.2 + n_2 h) \in \mathbb{R}^2 \mid n_1, n_2 \in \{0, 1, \dots, 300\} \} \cap \Omega,$$

with $h = 11/750$. We also consider the discrete \mathcal{L}^2 -error of a reconstruction \hat{f}_* defined as follows:

$$E_2(\hat{f}_*) := \left(\sum_{x \in \Omega_h} |f(x) - \hat{f}_*(x)|^2 \cdot h^2 \right)^{1/2}.$$

Let us discuss the reconstructions in Figure 6. First of all, as expected, one observes strong artifacts in the reconstruction \hat{f}_0 , especially outside of $\text{supp}(f)$. These artifacts are considerably corrected in the reconstruction $\hat{f}_{4 \times 2}$, and as the number of the training functions n increases, the artifacts become weaker such that the reconstruction $\hat{f}_{32 \times 16}$ is very similar to the reconstruction \hat{f} . This observation is also reflected in E_2 -errors that are presented in Figure 7. Note that \hat{f} differs from f due to the discretization error of the

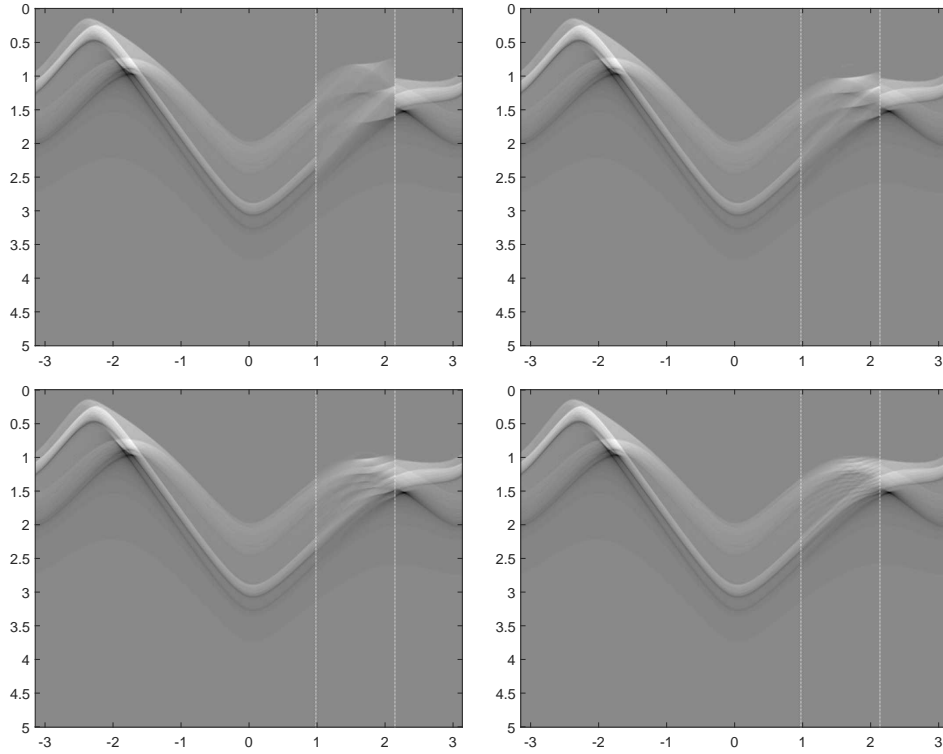


Figure 5: The extended limited view data \hat{u}_n using the learned extension operator $\hat{\mathcal{A}}_n$ for $n = 4 \times 2$, 8×4 , 16×8 , 32×16 (from left to right and from top to bottom). The gray scaling is as in Figure 3(right).

numerical realization of the formula \mathcal{G}_2 . Thus, as in the case of the data \hat{u}_n , the approach of \hat{f}_n to f is in agreement with Corollary 2.

Finally, in Table 1, we present the calculation times for the parts involved in the proposed reconstruction approach. Our numerical results are performed with MATLAB version R2015b on the PC lenovo e31 with four processors Intel(R) Xeon(R) CPU 3.20GHz. We see that the most time consuming part is the calculation of the matrix \mathbf{P}_n^{-1} , which is used for solving the system of linear equations (11). Here, the calculation of $u_{1,i} = \mathcal{U}_1 f_i$ is the most computationally expensive. But for a given set of the training functions f_i , $u_{1,i}$ and the matrix \mathbf{P}_n^{-1} have to be calculated only once and prior to the actual image reconstruction process.

The calculation of the learned data extension $\hat{\mathcal{A}}_n u_1$ is fast. In particular, for the biggest considered number $n = 32 \times 16$ of the training functions, the calculation time for $\hat{\mathcal{A}}_n u_1$ is near the calculation time for the formula \mathcal{G}_2 . Thus, our proposed operator learning approach fulfills the requirements that we stated at the beginning of Section 3.2. Namely, the closeness of the approximation $\hat{\mathcal{A}}_n u_1$ to $\mathcal{A} u_1$, and the fast evaluation of $\hat{\mathcal{A}}_n u_1$ are realized.

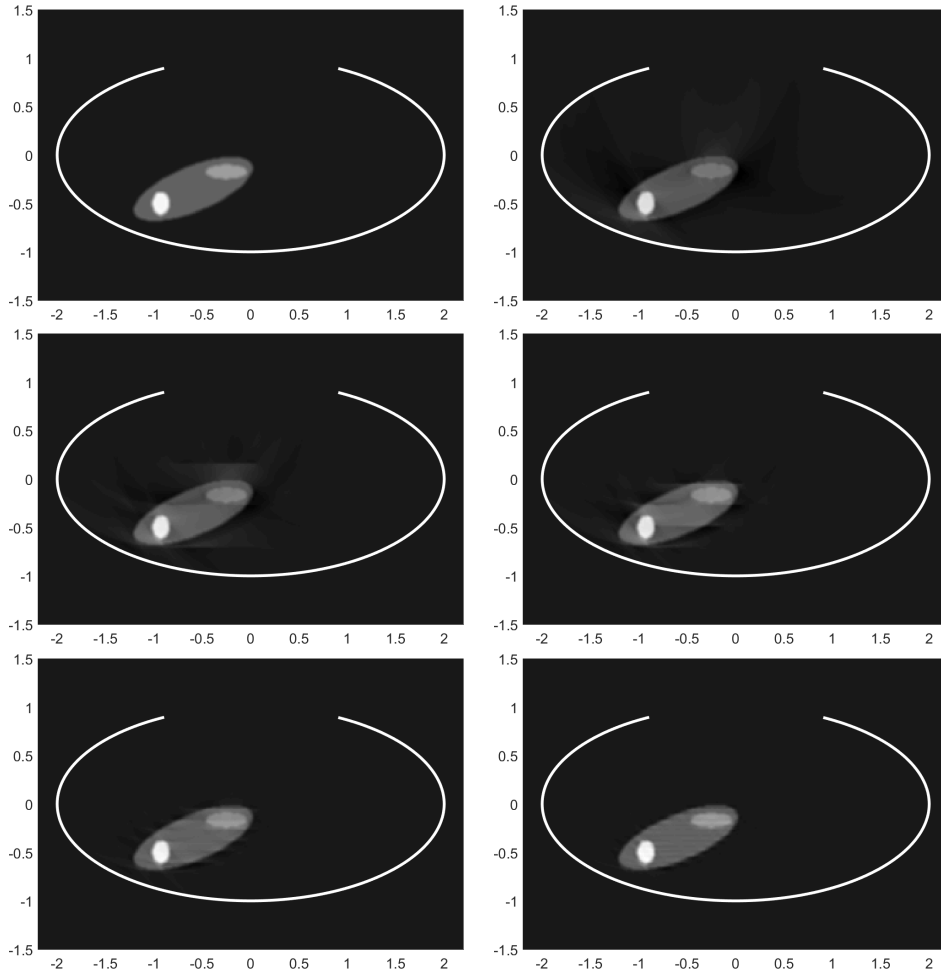


Figure 6: From left to right and from top to bottom: the reconstructions \hat{f} , \hat{f}_0 , and \hat{f}_n , for $n = 4 \times 2$, 8×4 , 16×8 , 32×16 . The gray scaling is as in Figure 3(left).

6 Conclusion and outlook

In this paper, we demonstrated that an approximate extension of the limited view data in PAT can be realized using an operator learning approach. Our numerical results show that the learned extension of the limited view data with a good approximation quality and a low computational cost is possible. A good approximation quality is especially achieved for the biggest number $n = 32 \times 16$ of considered training functions. This makes the proposed learned data extension attractive for the algorithms that are designed for the full view data. As an example, we demonstrated a satisfactory performance of a reconstruction formula with the proposed learned data extension.

It could be interesting to look at the behavior of the proposed learned data extension without knowledge of a rectangular region K containing $\text{supp}(f)$. As we already noted, in this case, one could consider partitions of the whole detection region Ω_1 . Also other training functions, such as generalized Kaiser-Bessel functions (see, e.g., [32, 46, 43]), can

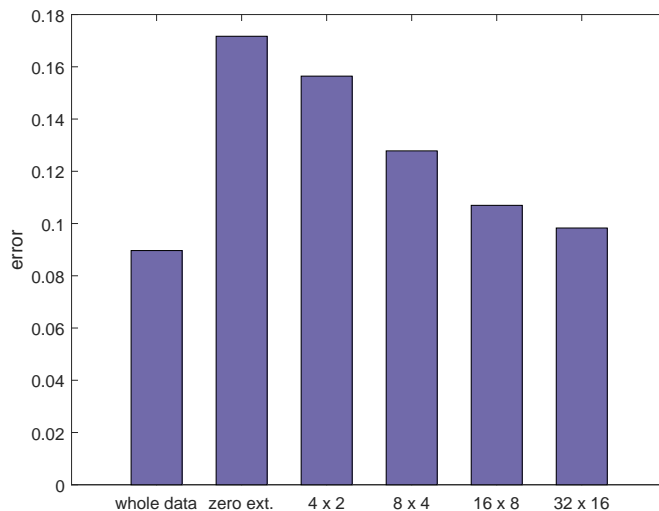


Figure 7: E_2 -errors of the considered reconstructions \hat{f} , \hat{f}_0 , and \hat{f}_n , for $n = 4 \times 2, 8 \times 4, 16 \times 8, 32 \times 16$.

Table 1: Calculation times in seconds for the parts involved in the proposed reconstruction approach.

n	\mathbf{P}_n^{-1}	$\hat{\mathcal{A}}_n u_1$	\mathcal{G}_2
4×2	1179.73	0.53	4.20
8×4	4707.31	0.68	3.55
16×8	19036.23	1.41	3.90
32×16	75874.87	6.07	4.33

be tried.

It is appealing to consider a comparison of the reconstruction quality and computation time of the proposed reconstruction approach and iterative reconstruction algorithms. Implementation of the proposed learned extension of the limited view data to three spatial dimensions is an interesting aspect of future research. In this case, the choice of the generalized Kaiser-Bessel functions as the training functions f_i is particularly convenient because for them the wave data $u_{1,i} = \mathcal{U}_1 f_i$, $u_{2,i} = \mathcal{U}_2 f_i$ are known analytically (see, e.g., [46]). This makes the determination of the entries of the matrix \mathbf{P}_n fast. Also, the solution of the system of linear equations (11) can be done either using iterative methods, such as conjugate gradient method, or an approximate inverse matrix to \mathbf{P}_n can be determined.

Finally, it seems to be worth to examine applications of the presented operator learning approach to the limited data problems in other tomographic modalities, such as sparse angle or region of interest computed tomography.

Acknowledgements

Authors gratefully acknowledge the support of the Tyrolean Science Fund (TWF). Sergiy Pereverzyev Jr. gratefully acknowledges the support of the Austrian Science Fund (FWF): project P 29514-N32. He also would like to thank Alessandro Verri, Vera Kurkova, Linh Nguyen, Jürgen Friel, Xin Guo, Ding-Xuan Zhou, and members of Ding-Xuan Zhou's group at the City University of Hong Kong for discussions concerning this work.

References

- [1] M. Agranovsky, D. Finch, and P. Kuchment. Range conditions for a spherical mean transform. *Inverse Probl. Imaging*, 3(3):373–383, 2009.
- [2] M. A. Alvarez, L. Rosasco, and N. D. Lawrence. Kernels for vector-valued functions: A review. *Found. Trends Mach. Learn.*, 4(3):195–266, 2012.
- [3] G. Ambartsoumian and P. Kuchment. A range description for the planar circular Radon transform. *SIAM J. Math. Anal.*, 38(2):681–692, 2006.
- [4] L. L. Barannyk, J. Friel, and L. V. Nguyen. On artifacts in limited data spherical Radon transform: curved observation surface. *Inverse Probl.*, 32(1):015012, 2015.
- [5] P. Beard. Biomedical photoacoustic imaging. *Interf. Focus*, 1(4):602–631, 2011.
- [6] P. Burgholzer, J. Bauer-Marschallinger, H. Grün, M. Haltmeier, and G. Paltauf. Temporal back-projection algorithms for photoacoustic tomography with integrating line detectors. *Inverse Probl.*, 23(6):S65–S80, 2007.
- [7] P. Burgholzer, G. J. Matt, M. Haltmeier, and G. Paltauf. Exact and approximate imaging methods for photoacoustic tomography using an arbitrary detection surface. *Phys. Rev. E*, 75(4):046706, 2007.
- [8] R. Courant and D. Hilbert. *Methods of Mathematical Physics. Volume 2*. Wiley-Interscience, New York, 1962.
- [9] D. Finch, M. Haltmeier, and Rakesh. Inversion of spherical means and the wave equation in even dimensions. *SIAM J. Appl. Math.*, 68(2):392–412, 2007.
- [10] D. Finch, S. Patch, and Rakesh. Determining a function from its mean values over a family of spheres. *SIAM J. Math. Anal.*, 35(5):1213–1240, 2004.
- [11] D. Finch and Rakesh. The range of the spherical mean value operator for functions supported in a ball. *Inverse Probl.*, 22(3):923–938, 2006.
- [12] D. Finch and Rakesh. Recovering a function from its spherical mean values in two and three dimensions. In L. V. Wang, editor, *Photoacoustic imaging and spectroscopy*, chapter 7, pages 77–88. CRC Press, 2009.
- [13] J. Friel and E. T. Quinto. Characterization and reduction of artifacts in limited angle tomography. *Inverse Probl.*, 29(12):21, 2013.

- [14] J. Friel and E. T. Quinto. Artifacts in incomplete data tomography with applications to photoacoustic tomography and sonar. *SIAM J. Appl. Math.*, 75(2):703–725, 2015.
- [15] H. Grün, T. Berer, P. Burgholzer, R. Nuster, and G. Paltauf. Three-dimensional photoacoustic imaging using fiber-based line detectors. *J. Biomed. Optics*, 15(2):021306, 2010.
- [16] M. Haltmeier. Frequency domain reconstruction for photo- and thermoacoustic tomography with line detectors. *Math. Mod. Meth. Appl. Sci.*, 19(2):283–306, 2009.
- [17] M. Haltmeier. Inversion of circular means and the wave equation on convex planar domains. *Comput. Math. Appl.*, 65(7):1025–1036, 2013.
- [18] M. Haltmeier. Universal inversion formulas for recovering a function from spherical means. *SIAM J. Math. Anal.*, 41(1):214–232, 2014.
- [19] M. Haltmeier and L. V. Nguyen. Analysis of iterative methods in photoacoustic tomography with variable sound speed. *SIAM J. Imaging Sci.*, 10(2):751–781, 2017.
- [20] M. Haltmeier and S. Pereverzyev Jr. Recovering a function from circular means or wave data on the boundary of parabolic domains. *SIAM J. Imaging Sci.*, 8(1):592–610, 2015.
- [21] M. Haltmeier and S. Pereverzyev Jr. The universal back-projection formula for spherical means and the wave equation on certain quadric hypersurfaces. *J. Math. Anal. Appl.*, 429(1):366–382, 2015.
- [22] T. Hastie, R. Tibshirani, and J. Friedman. *The Elements of Statistical Learning*. Springer Series in Statistics, 2009.
- [23] G. T. Herman. *Fundamentals of computerized tomography: image reconstruction from projections*. Springer, 2009.
- [24] Y. Hristova, P. Kuchment, and L. Nguyen. Reconstruction and time reversal in thermoacoustic tomography in acoustically homogeneous and inhomogeneous media. *Inverse Probl.*, 24(5):055006 (25pp), 2008.
- [25] C. Huang, K. Wang, L. Nie, L. V. Wang, and M. A. Anastasio. Full-wave iterative image reconstruction in photoacoustic tomography with acoustically inhomogeneous media. *IEEE Trans. Med. Imaging*, 32(6):1097–1110, 2013.
- [26] P. Kuchment and L. Kunyansky. Mathematics of photoacoustic and thermoacoustic tomography. In *Handbook of Mathematical Methods in Imaging*, pages 817–865. Springer, 2011.
- [27] P. Kuchment and L. A. Kunyansky. Mathematics of thermoacoustic and photoacoustic tomography. *Eur. J. Appl. Math.*, 19:191–224, 2008.
- [28] L. A. Kunyansky. Explicit inversion formulae for the spherical mean Radon transform. *Inverse Probl.*, 23(1):373–383, 2007.
- [29] L. A. Kunyansky. A series solution and a fast algorithm for the inversion of the spherical mean Radon transform. *Inverse Probl.*, 23(6):S11–S20, 2007.

- [30] L. A. Kunyansky. Reconstruction of a function from its spherical (circular) means with the centers lying on the surface of certain polygons and polyhedra. *Inverse Probl.*, 27(2):025012, 2011.
- [31] C. Li and L. V. Wang. Photoacoustic tomography and sensing in biomedicine. *Phys. Med. Biol.*, 54(19):R59, 2009.
- [32] S. Matej and R. M. Lewitt. Practical considerations for 3-D image reconstruction using spherically symmetric volume elements. *IEEE Trans. Med. Imag.*, 15(1):68–78, 1996.
- [33] C. A. Micchelli and M. Pontil. On learning vector-valued functions. *Neural Comput.*, 17(1):177–204, 2005.
- [34] F. Natterer. Photo-acoustic inversion in convex domains. *Inverse Probl. Imaging*, 6(2):315–320, 2012.
- [35] L. V. Nguyen. On a reconstruction formula for spherical Radon transform: A microlocal analytic point of view. *Anal. Math. Phys.*, 4(3):199–220, 2014.
- [36] L. V. Nguyen. On artifacts in limited data spherical Radon transform: flat observation surfaces. *SIAM J. Math. Anal.*, 47(4):2984–3004, 2015.
- [37] G. Paltauf, R. Nuster, M. Haltmeier, and P. Burgholzer. Experimental evaluation of reconstruction algorithms for limited view photoacoustic tomography with line detectors. *Inverse Probl.*, 23(6):S81–S94, 2007.
- [38] G. Paltauf, R. Nuster, M. Haltmeier, and P. Burgholzer. Photoacoustic tomography using a Mach-Zehnder interferometer as an acoustic line detector. *App. Opt.*, 46(16):3352–3358, 2007.
- [39] G. Paltauf, J. A. Viator, S. A. Prahl, and S. L. Jacques. Iterative reconstruction algorithm for optoacoustic imaging. *J. Acoust. Soc. Am.*, 112(4):1536–1544, 2002.
- [40] S. K. Patch. Thermoacoustic tomography — consistency conditions and the partial scan problem. *Phys. Med. Biol.*, 49:2305–2315, 2004.
- [41] S. K. Patch. Photoacoustic and thermoacoustic tomography: Consistency conditions and the partial scan problem. In *Photoacoustic Imaging and Spectroscopy*, pages 103–116. CRC Press, 2009.
- [42] A. Rosenthal, V. Ntziachristos, and D. Razansky. Acoustic inversion in optoacoustic tomography: A review. *Curr. Med. Imaging Rev.*, 9(4):318–336, 2013.
- [43] J. Schwab, S. Pereverzyev Jr., and M. Haltmeier. A Galerkin least squares approach for photoacoustic tomography. Technical report, University of Innsbruck, Department of Mathematics, Applied Mathematics Group, 2017. Preprint Nr. 30, arXiv:1612.08094 [math.NA].
- [44] P. Stefanov and G. Uhlmann. Thermoacoustic tomography with variable sound speed. *Inverse Probl.*, 25(7):075011, 2009.

- [45] P. Stefanov and G. Uhlmann. Is a curved flight path in SAR better than a straight one? *SIAM J. Appl. Math.*, 73(4):1596–1612, 2013.
- [46] K. Wang, R. W. Schoonover, R. Su, A. Oraevsky, and M. A. Anastasio. Discrete imaging models for three-dimensional optoacoustic tomography using radially symmetric expansion functions. *IEEE Trans. Med. Imag.*, 33(5):1180–1193, 2014.
- [47] J. Xia, J. Yao, and L. V. Wang. Photoacoustic tomography: principles and advances. *Prog. Electromagnetics Res.*, 147:1–22, 2014.
- [48] M. Xu and L. V. Wang. Universal back-projection algorithm for photoacoustic computed tomography. *Phys. Rev. E*, 71(1):0167061–0167067, 2005.
- [49] M. Xu and L. V. Wang. Photoacoustic imaging in biomedicine. *Rev. Sci. Instruments*, 77(4):041101 (22pp), 2006.
- [50] Y. Xu, L. V. Wang, G. Ambartsoumian, and P. Kuchment. Reconstructions in limited-view thermoacoustic tomography. *Med. Phys.*, 31(4):724–733, 2004.
- [51] Y. Xu, M. Xu, and L. V. Wang. Exact frequency-domain reconstruction for thermoacoustic tomography–II: Cylindrical geometry. *IEEE Trans. Med. Imag.*, 21:829–833, 2002.
- [52] L. Yao and H. Jiang. Photoacoustic image reconstruction from few-detector and limited-angle data. *Biomed. Opt. Express*, 2(9):2649–2654, 2011.
- [53] G. Zangerl, O. Scherzer, and M. Haltmeier. Exact series reconstruction in photoacoustic tomography with circular integrating detectors. *Commun. Math. Sci.*, 7(3):665–678, 2009.